Earth and Planetary Science Letters 399 (2014) 61–73

Contents lists available at ScienceDirect

Earth and Planetary Science Letters

www.elsevier.com/locate/epsl

Sulfur and oxygen isotope fractionation during sulfate reduction coupled to anaerobic oxidation of methane is dependent on methane concentration

Christian Deusner [a,b,*], Thomas Holler [a], Gail L. Arnold [c,d], Stefano M. Bernasconi [e], Michael J. Formolo [a,f], Benjamin Brunner [a,c,d,*]

[a] Max Planck Institute for Marine Microbiology, Bremen, Germany
[b] GEOMAR Helmholtz Centre for Ocean Research Kiel, Kiel, Germany
[c] Center for Geomicrobiology, Department of Bioscience, Aarhus University, Denmark
[d] Department of Geosciences, University of Texas at El Paso, TX, USA
[e] Geological Institute, ETH Zürich, Zürich, Switzerland
[f] Department of Geosciences, The University of Tulsa, Tulsa, OK, USA

ARTICLE INFO

Article history:
Received 13 September 2013
Received in revised form 29 April 2014
Accepted 30 April 2014
Available online 27 May 2014
Editor: G.M. Henderson

Keywords:
anaerobic oxidation of methane (AOM)
sulfate reduction
sulfur disproportionation
sulfur isotope fractionation
oxygen isotope fractionation
thermodynamics and reversibility

ABSTRACT

Isotope signatures of sulfur compounds are key tools for studying sulfur cycling in the modern environment and throughout earth's history. However, for meaningful interpretations, the isotope effects of the processes involved must be known. Sulfate reduction coupled to the anaerobic oxidation of methane (AOM-SR) plays a pivotal role in sedimentary sulfur cycling and is the main process responsible for the consumption of methane in marine sediments – thereby efficiently limiting the escape of this potent greenhouse gas from the seabed to the overlying water column and atmosphere. In contrast to classical dissimilatory sulfate reduction (DSR), where sulfur and oxygen isotope effects have been measured in culture studies and a wide range of isotope effects has been observed, the sulfur and oxygen isotope effects by AOM-SR are unknown. This gap in knowledge severely hampers the interpretation of sulfur cycling in methane-bearing sediments, especially because, unlike DSR which is carried out by a single organism, AOM-SR is presumably catalyzed by consortia of archaea and bacteria that both contribute to the reduction of sulfate to sulfide.

We studied sulfur and oxygen isotope effects by AOM-SR at various aqueous methane concentrations from 1.4 ± 0.6 mM up to 58.8 ± 10.5 mM in continuous incubation at steady state. Changes in the concentration of methane induced strong changes in sulfur isotope enrichment (ε^{34}S) and oxygen isotope exchange between water and sulfate relative to sulfate reduction (θ_O), as well as sulfate reduction rates (SRR). Smallest ε^{34}S (21.9 ± 1.9‰) and θ_O (0.5 ± 0.2) as well as highest SRR were observed for the highest methane concentration, whereas highest ε^{34}S (67.3 ± 26.1‰) and θ_O (2.5 ± 1.5) and lowest SRR were reached at low methane concentration. Our results show that ε^{34}S, θ_O and SRR during AOM-SR are very sensitive to methane concentration and thus also correlate with energy yield. In sulfate–methane transition zones, AOM-SR is likely to induce very large sulfur isotope fractionation between sulfate and sulfide (i.e. >60‰) and will drive the oxygen isotope composition of sulfate towards the sulfate–water oxygen isotope equilibrium value. Sulfur isotope fractionation by AOM-SR at gas seeps, where methane fluxes are high, will be much smaller (i.e. 20 to 40‰).

1. Introduction

1.1. Sulfur and oxygen isotopes as tracers of present and past environmental processes

Sulfur isotopes are essential for the reconstruction of sulfur cycling through earth's history. They have been used to explore

* Corresponding authors.
E-mail addresses: cdeusner@geomar.de (C. Deusner), bbrunner@utep.edu (B. Brunner).

http://dx.doi.org/10.1016/j.epsl.2014.04.047
0012-821X/

themes such as Earth's early atmosphere (Farquhar et al., 2000; Ono et al., 2005), the antiquity of sulfate reduction (Philippot et al., 2007; Shen et al., 2009), the evolution of atmospheric oxygen content over the Phanerozoic (Berner et al., 2000), and biogeochemical sulfur cycling over a broad range of geological time periods (e.g. Burdett et al., 1989; Canfield and Teske, 1996; Paytan et al., 1998; Ohkouchi et al., 1999; Kampschulte et al., 2001; Strauss et al., 2001; Paytan et al., 2004; Johnston et al., 2005; Wortmann and Chernyavsky, 2007; for a review see Bottrell and Newton, 2006). In recent years, it has become evident that the oxygen isotope composition of sulfate provides information on oxidative processes within the sulfur cycle that cannot be elucidated by the analysis of sulfur isotopes alone (Turchyn and Schrag, 2004). The study of the oxygen isotope composition of sulfate has turned out to be crucial for the understanding of deep biosphere sulfur cycling (Böttcher et al., 1998, 2000; Wortmann et al., 2007; Riedinger et al., 2010; Antler et al., 2013), oxidative sulfur cycling at the sediment-water interface (Ku et al., 1999; Böttcher and Thamdrup, 2001; Böttcher et al., 2001), the exploration of the formation of phosphatic laminites (Arning et al., 2009) and diagenetic gypsum (Pierre, 1985; Pirlet et al., 2010). Furthermore, the oxygen isotope composition of sulfate has been found to be a useful tool for evaluating sulfur cycling in soils and aquifers contaminated with aromatic hydrocarbons (Knöller et al., 2006, 2008), as well as for fingerprinting of microbial activity in acid mine drainage (e.g. Balci et al., 2007; Brunner et al., 2008; Heidel and Tichomirowa, 2011; Müller et al., 2013).

1.2. Sulfate reduction coupled to the anaerobic oxidation of methane

Sulfate reduction coupled to the anaerobic oxidation of methane (AOM-SR) is considered a process of worldwide relevance, because it is responsible for methane consumption in anoxic marine environments and thereby limits the escape of this potent greenhouse gas from the seabed (Reeburgh, 2007). Availability of dissolved methane regulates AOM-SR, with maximum solubility of methane being dependent mainly on pressure and temperature conditions. Consequently, methane availability varies strongly between different sites where AOM-SR is active, which can be gas seeps, mud volcanoes, hydrate fields or marine sediments rich in organic matter (Knittel and Boetius, 2009). Additionally, at sites where AOM-SR occurs, methane concentrations can vary strongly depending on spatial and temporal variations in methane supply and microbial turnover rates. Allegedly, AOM-SR is catalyzed by syntrophic consortia of methanotrophic archaea (ANME) that generally appear to operate in concert with *Desulfosarcina*-like (DSS) bacterial partners belonging to the *Deltaproteobacteria* class (for review, see Knittel and Boetius, 2009) according to the net reaction:

$$CH_4 + SO_4^{2-} \rightarrow HCO_3^- + HS^- + H_2O$$
$$\Delta G^0 = -16.6\ \mathrm{kJ/mol} \qquad (1)$$

Recently Milucka et al. (2012) proposed that AOM-SR may be carried out by the ANME and not (only) by their bacterial partners and suggested that the ANME reduce sulfate to zero-valent sulfur, which is disproportionated to sulfate and sulfide by the DSS (Fig. 1b). Immuno-assay studies of the same AOM consortium found no indication that the ANME possess ATP sulfurylase (Sat) or dissimilatory sulfite reductase (Dsr), key enzymes of the classic pathways to activate sulfate to APS and to produce the final product, sulfide (Milucka et al., 2012).

The possibility that ANME use an alternative sulfate reduction pathway to canonical DSR and partner with sulfur disproportionating DSS that likely use the canonical DSR pathway by partially operating it in reverse direction (Frederiksen and Finster, 2003; Finster et al., 2013; Fig. 1) raises the question if the relationship between sulfur and oxygen isotope fractionation observed for AOM-SR may be similar to the observed relationship for DSR, despite the differences in metabolic pathways.

1.3. Sulfur and oxygen isotope effects by DSR – the links between reversibility, energy yield and sulfate reduction rate

Sulfur isotope enrichment effects ($\varepsilon^{34}S$) reported for DSR cover a wide range from observations of $-3‰$ to the theoretical sulfur isotope equilibrium between sulfate and sulfide at $+75‰$, or even higher (for a review, see Sim et al., 2011a). The oxygen isotope effects by DSR are somewhat more subtle, driving the oxygen isotope composition of sulfate towards the isotope equilibrium fractionation value between sulfate and water (Mizutani and Rafter, 1969; Fritz et al., 1989; Brunner et al., 2005) of approximately $\sim 28‰$ at 4 °C (Zeebe, 2010). There are also cases where no oxygen isotope fractionation was detected (Turchyn et al., 2010).

Sulfur and oxygen isotope effects during DSR are the result of a sequence of isotope effects intrinsic to enzymatically-catalyzed steps in the sulfate reduction cascade and of the reversibility of this process (Fig. 1a). The extent to which these intrinsic isotope effects are expressed as overall isotope fractionation by DSR depends on how much back flux relative to the forward flux (i.e. reversibility) occurs in single steps (e.g. Rees, 1973; Brüchert, 2004; Brunner and Bernasconi, 2005; Farquhar et al., 2008; Bradley et al., 2011). The effects of increasing reversibility are two-fold. First, the sulfur isotope offset (expressed as $\varepsilon^{34}S$) between substrate sulfate and produced sulfide increases. Second, the oxygen isotope exchange between sulfate and water, mediated by rapid oxygen isotope exchange between sulfur-oxy intermediates in the DSR pathway, relative to the sulfate reduction rate (overall expressed as θ_O, see Brunner et al., 2012 and references therein) also increases.

The reversibility of DSR has long since been recognized as the main controlling factor for the expression of sulfur and oxygen isotope effects, while the parameters that control the reversibility of the DSR network and its individual steps remain less certain. Nevertheless, it is evident that ultimately, thermodynamics control the reversibility of individual biochemical reactions, and thereby the reversibility of a sequence of such steps. This can best be exemplified for a simple enzymatic reaction from a substrate to a product ($A \rightarrow P$). The reversibility is given by the relationship

$$\frac{f_-}{f_+} = \frac{[P]}{K_e \cdot [A]} = e^{\Delta G/(R \cdot T)} \qquad (2)$$

where f_- and f_+ denote back and forward flux, K_e the equilibrium constant ($K_e = e^{-\Delta G/(R \cdot T)}$), and ΔG the free energy of the reaction (for a discussion, see Holler et al., 2011a). The net flux (f_{net}) is given as

$$f_{net} = f_+ - f_- = f_+ \cdot \left(1 - \frac{[P]}{K_e \cdot [A]}\right) = f_+ \cdot \left(1 - e^{\Delta G/(R \cdot T)}\right) \qquad (3)$$

Eqs. (2) and (3) show that if the free energy of the reaction is small, which is the case when the reaction approaches thermodynamic equilibrium, reversibility becomes large (i.e. close to unity) while f_{net} becomes small (i.e. close to zero). The above equations do not imply that thermodynamics govern kinetics; they merely state that for a certain reaction rate (i.e., f_+), thermodynamics determine the rate in the opposite direction (i.e., f_-).

Intuitively, one also expects that reaction rates control the expression of isotope effects: reaction steps in DSR that proceed rapidly are assumed to deplete internal sulfur-oxy pools and

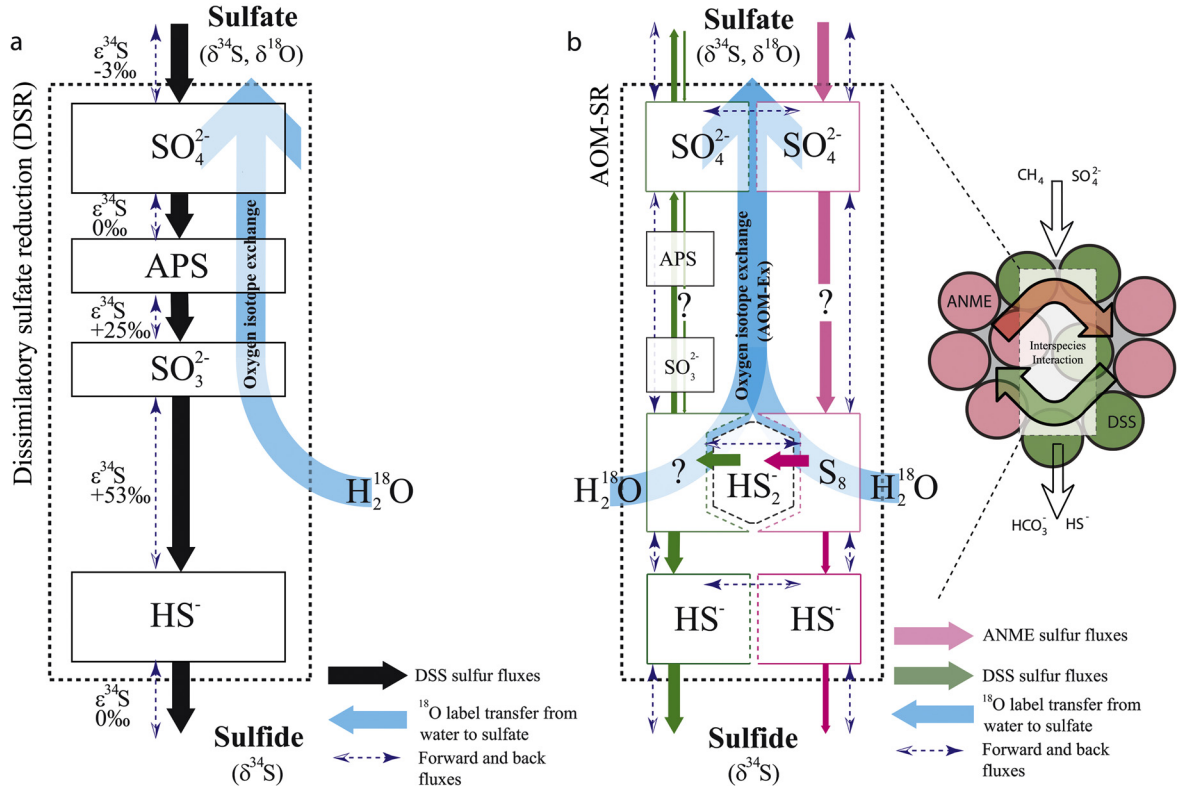

Fig. 1. Scheme of AOM-SR and putative mass and isotope fluxes in DSR. (a) Mass fluxes, sulfur isotope fractionation and oxygen isotope exchange for DSR. In DSR, extracellular sulfate is transported into the cell and subsequently reduced to sulfide via sulfur-oxy intermediates such as adenosine phosphosulfate (APS) and sulfite. The sulfur isotope enrichment fractionation factors $\varepsilon^{34}S_{APS-sulfite}$ and $\varepsilon^{34}S_{sulfite-sulfide}$ are assumed to be +25‰ and +53‰, respectively. The DSR pathway is reversible and the ratio of individual forward and backward fluxes is assumed to be thermodynamically controlled. Oxygen isotope exchange between water and sulfate is mediated via oxygen isotope exchange between water and sulfite and subsequent back flux to sulfate. (b) AOM-SR is purportedly catalyzed by two phylogenetically distinct partner organisms – ANME and DSS – in a syntrophic consortium. Recently, it was proposed that likely both organisms are involved in the reduction of sulfate to sulfide, where the ANME partner reduces sulfate to zero-valent sulfur by an unknown pathway and the DSS partner disproportionates zero-valent sulfur to sulfide and back into sulfate (Milucka et al., 2012), potentially by partially reversing the DSR pathway. Probably, zero-valent sulfur is shuttled from the ANME to the DSS in the form of disulfide (HS_2^-).

thereby limit the back-flow of isotopically altered sulfur compounds which leads to a suppression of the intrinsic isotope effects, leading to the conclusion that there should be a link between sulfur and oxygen isotope fractionation and SRR (Böttcher et al., 1998, 1999; Sim et al., 2011b and references therein; Antler et al., 2013; Leavitt et al., 2013). Postulating a relationship between SRR and sulfur and oxygen isotope effects ignores that a back reaction may scale with the forward reaction, keeping the ratio between the fluxes constant, but increasing the observed net reaction. Such a scenario is given when DSR cultures grow, a reason why, typically, $\varepsilon^{34}S$ and θ_O are compared to cell specific sulfate reduction rates (SRR_{cs}; Harrison and Thode, 1958; Chambers et al., 1975; Chambers and Trudinger, 1979; Canfield, 2001; Detmers et al., 2001; Kleikemper et al., 2004; Johnston et al., 2007; Turchyn et al., 2010; Sim et al., 2011b). Even the normalization of SRR to cell numbers may not resolve this issue entirely, because sulfate reducing microorganisms can increase their pool of enzymes, thereby changing SRR_{cs} without affecting $\varepsilon^{34}S$ or θ_O. Nevertheless, a compilation by Sim et al. (2011b) showed that there is correlation between $\varepsilon^{34}S$ and SRR_{cs}, which appears to be species-specific. Furthermore, experiments with batch cultures of *Desulfovibrio* sp. DMSS-1 provided with different electron donors and experiments with continuous cultures of *D*. sp. DMSS-1 under different concentrations of lactate reveal that low SRR_{cs} and high $\varepsilon^{34}S$ coincide with refractory organic substrates and substrate limitation whereas high SRR_{cs} and low $\varepsilon^{34}S$ coincide with easily degradable substrates and at high substrate concentrations. These findings were corroborated by Leavitt et al. (2013) who observed that $\varepsilon^{33}S$ and $\varepsilon^{34}S$ by the sulfate reducing bacterium *Desulfovibrio vulgaris* Hildenborough increase when lactate concentrations decrease, leading to the hypothesis that combined ^{33}S–^{34}S signatures could be a proxy to reconstruct environmental sulfate reduction rates in the geologic past.

1.4. Sulfur and oxygen isotope effects of sulfate reduction coupled to the anaerobic oxidation of methane

So far, direct measurements of the sulfur and oxygen isotope effects of AOM-SR in culture are lacking. Sulfur isotope trends from sulfate, sulfide, and sulfide minerals obtained from marine sediments close to active or past sulfate–methane transition zones (SMTZs) indicate that similar to DSR, AOM-SR produces sulfide that is depleted in ^{34}S relative to sulfate (e.g. Böttcher et al., 2003; Jørgensen et al., 2004; Borowski et al., 2013). Judging from the scarce oxygen isotope data available for natural environments that may have been affected by AOM-SR (i.e. where sulfate concentrations reach depletion; Aharon and Fu, 2000, 2003; Antler et al., 2013) there is no oxygen isotope signature for AOM-SR that is distinct from the isotope signature of DSR.

While the details of the biochemical reactions and couplings of AOM-SR remain unresolved (Milucka et al., 2012; Fig. 1), it is obvious that the overall process has a low energy yield (Eq. (1)), which is shared between the microorganisms that form the consortium. Sulfate reduction, methane oxidation, and each individual enzymatic reaction are expected to operate very close to thermodynamic equilibrium and thus must operate reversibly, a concept recently tested for AOM-SR. Yoshinaga et al. (2014) showed that enzymatic reversibility in AOM at low substrate concentra-

tions strongly influences carbon isotope signatures of methane and dissolved inorganic carbon. Holler et al. (2011a) previously found that cultures of highly enriched AOM consortia converted labeled catabolic products ^{14}C-bicarbonate and ^{35}S-sulfide to ^{14}C-methane and ^{35}S-sulfate, respectively, thus indicating full process reversibility. However, there remains the caveat that ^{35}S label transfer from sulfide to sulfate does not unambiguously prove the full reversibility of sulfur transformations carried out by the ANME, as abiotic sulfur isotope exchange between ^{35}S sulfide and zero-valent sulfur followed by sulfur disproportionation by DSS, as lately postulated by Milucka et al. (2012), could be responsible for the formation of ^{35}S sulfate. Nevertheless, under typical thermodynamic constraints for AOM-SR, the reversibility of sulfur transformations should be high and strongly depend on methane concentrations (Eq. (2)). We, therefore, expect to observe a strong dependency of ε^{34}S and θ_O of AOM-SR to methane concentrations, with large sulfur isotope fractionation up to the theoretical value of approximately 75‰ and rapid oxygen isotope exchange between sulfate and water relative to the SSR at low methane concentrations.

2. Materials and methods

2.1. Organisms and medium composition

Biomass slurries were prepared from naturally enriched environmental samples of microbial mats from Black Sea microbial reefs at 44°46′N, 31°59′E (*RV Meteor* cruise M72/2, 2007, Project MUMM, Max Planck Institute for Marine Microbiology, Bremen). For a microbiological and molecular characterization of the mats see Basen et al. (2011). After recovery the samples were stored under methanotrophic conditions with 0.2 MPa of methane in anoxic artificial seawater (Widdel and Bak, 1992). During storage, AOM-SR activity was monitored by measuring sulfide production. Medium was exchanged on a weekly basis to avoid inhibition of AOM-SR by sulfide accumulation. All manipulations of biomass were carried out under anoxic conditions. Mat pieces were homogenized using a tissue grinder prior to use in the experiments. The incubations were carried out at 20 °C with anoxic artificial seawater medium. Artificial seawater medium with sulfate (~8 mM between 0 and 110 days, ~10 mM between 110 and 129 days) was prepared with ammonium (4 mM), phosphate (1 mM), trace elements, vitamins, bicarbonate (30 mM) and sulfide (0.5 mM) after (Widdel and Bak, 1992). Sulfate concentrations were adjusted to relatively low values as compared to seawater composition to facilitate measurements of changes in the sulfur and oxygen isotope composition of sulfate (δ^{34}S, δ^{18}O, respectively) at low overall turnover rates. However, sulfate concentrations were well within the range of natural concentrations, which were measured to be as low as 6 mM in microbial mat chimneys in the Black Sea (Arnds, 2009). Prior to incubation the medium was spiked with ^{18}O-water (+610‰ vs. VSMOW). This amendment is necessary to obtain reliable values for θ_O, but comes at the price that a direct comparison to environmental data is no longer possible (i.e. due to a much higher equilibrium value). The dry weight (DW) was determined at the start of the long-term incubation experiment from an aliquot of 10 mL inoculated medium containing homogenized microbial mat samples which was dried at 80 °C for 24 h after separation from the fluid by centrifugation (10 000 rpm). The initial biomass dry weight concentration was 4.6 $g_{DW}\,L^{-1}$. Due to the strong tendency for biomass aggregation and sedimentation, and the very low dilution rates (D = flux/incubation reactor volume) of 1.7 d^{-1}, the biomass was completely retained within the incubation vessel during long-term incubation.

2.2. High pressure incubations, apparatus and sampling

To carry out the AOM-SR experiments at different methane concentrations we used a two stage high-pressure continuous incubation experimental system (HP-CI, see Fig. 2 for setup scheme). A detailed description of the HP-CI system is given in Deusner et al. (2010). All experiments presented here were carried out in continuous operation at steady state to allow for repeated measurements, particularly at low methane concentrations. The two-stage HP-CI system consists of pressure vessels for gas enrichment and biomass incubation. Biomass incubation was carried out at a constant hydrostatic pressure of 15 MPa to avoid effects of pressure changes on the culture. Liquid samples during continuous operation of the HP-CI system were taken directly into glass vials closed with butyl stoppers from the medium reservoir bottle and downstream of both reaction vessels for gas enrichment and biomass incubation, respectively, at sampling ports (Fig. 2). Samples for sulfide and sulfate (concentration and isotope composition) were collected directly into closed vials that contained zinc acetate solution (5% w/v), which prevents loss of gaseous hydrogen sulfide that might out-gas together with methane if sampling was done into open vials. Samples for methane concentrations were collected into closed vials containing a saturated sodium chloride solution. The methane concentration was measured from the headspace of the sampling vials.

The total duration of high-pressure biomass incubation was 129 days (February 2009–June 2009). During this period the influent concentration of aqueous methane was stepwise increased from 1.4 ± 0.6 mM to 58.8 ± 10.5 mM, with intervals of batch incubation, flushing and stabilization between measurement periods. During stabilization intervals the bioreactor system was first flushed at fourfold increased flow rate (2 mL/min instead of 0.5 mL/min during measurement intervals) and after that operated at the respective incubation conditions for at least 42 h prior to each measurement period. The system was judged to be at steady state when the reactor incubation volume (420 mL) was exchanged at least three times at the respective methane concentration and flow rate. Once steady state was reached, several samples were taken without biomass depressurization and the system was subsequently adjusted to a higher methane concentration. At each methane concentration step, incubation was carried out for 1.8 to 6.2 days, with repeated sampling and analysis of influent and effluent fluids from the incubation vessel.

2.3. Measurement of sulfate, sulfide and methane concentrations

Precipitated zinc sulfide was re-suspended and the total sulfide concentration (here abbreviated as [HS^-]) was determined colorimetrically according to the methylene-blue reaction in a miniaturized assay (Aeckersberg et al., 1991). The sulfate concentration ([SO_4^{2-}]) was measured from the sample supernatant with ion chromatography with a SYKAM Solvent Delivery System coupled to a Millipore Waters Conductivity Detector Model 430 and a Waters IC PAK column or a Metrohm Advanced Compact IC 761 equipped with an electrical conductivity detector and a Metrosep A Supp 5–50 column. Methane concentrations were determined with a GC 14B gas chromatograph (Shimadzu) equipped with a Supel-Q Plot column (30 m × 0.53 mm; Supelco) and a flame ionization detector. The carrier gas was N_2 at a flow rate of 3 $mL\,min^{-1}$. The column temperature was 110 °C.

2.4. Isotope analysis

Sulfate was precipitated with an acidified barium chloride ($BaCl_2$) solution as barium sulfate ($BaSO_4$). The $BaSO_4$ precipitate

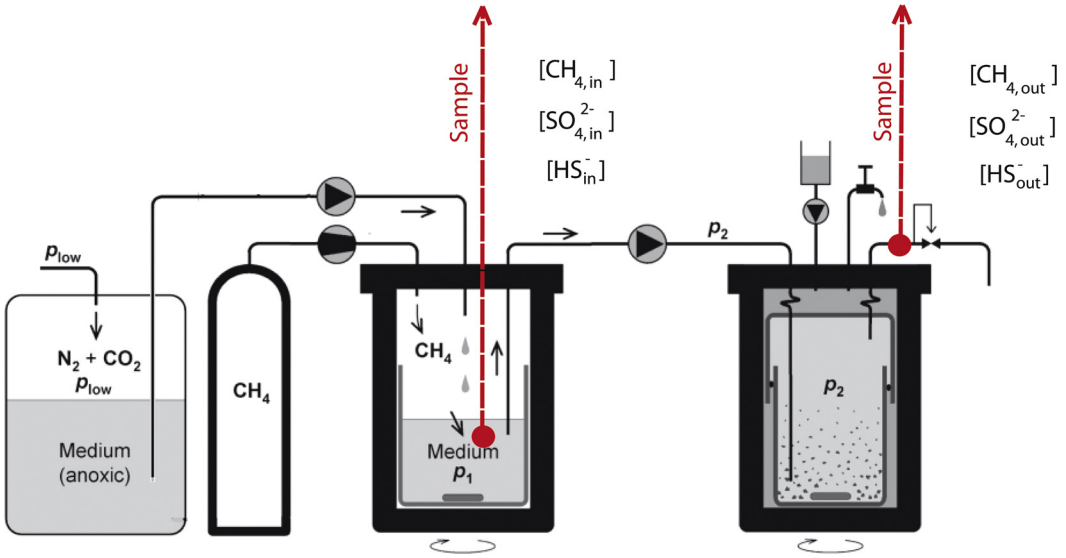

Fig. 2. High pressure flow-through incubation system. Two-stage experimental system for high pressure continuous incubation experiments (Deusner et al., 2010). Anoxic medium is delivered at a constant rate with a high pressure pump into the gas saturation vessel which is pressurized with methane to a desired pressure (p_1). Continuously stirred medium is rapidly enriched with methane according to the pressure–temperature conditions. The methane-enriched medium is delivered with a second pump into the incubation vessel. The pressure (p_2) inside the incubation vessel is regulated with a backpressure valve downstream of the vessel. To prevent effects from corrosion of the high-pressure components, both pressure vessels were equipped with internal PEEK containers. Samples of influent and effluent sulfate, sulfide and methane were taken upstream and downstream of the incubation vessel. Sampling points are shown in red. (For interpretation of the references to color in this figure legend, the reader is referred to the web version of this article.)

was recovered by centrifugation, where the supernatant was decanted. Samples were two times re-suspended with de-ionized water, followed by centrifugation. Subsequently, the $BaSO_4$ was re-dissolved with a strong chelator (DTPA, Bao, 2006) to liberate water from the medium (enriched in ^{18}O) that is potentially trapped in the $BaSO_4$ precipitate. The $BaSO_4$ was re-precipitated by addition of acidified barium chloride ($BaCl_2$) solution, washed with de-ionized water and dried at 50 °C for at least 24 h. Zinc sulfide was converted into silver sulfide (Ag_2S) with a silver nitrate ($AgNO_3$) solution. The precipitate was rinsed with de-ionized water and washed with 1 M NH_4OH solution to remove any silver chloride. After repeating the rinse step with de-ionized water the precipitate was dried at 50 °C overnight. Sulfur and oxygen isotope measurements of solid samples were performed with a gas source stable isotope ratio mass spectrometer (GS-IRMS) model Delta^{PLUS} (Finnigan; Thermo Fisher Scientific, Waltham, MA, USA) at the Max Planck Institute for Marine Microbiology in Bremen, Germany. The sulfur isotopic composition is reported with respect to the Vienna Cañon Diablo Troilite (VCDT) standard. The sulfur isotope measurements were calibrated with reference materials NBS 127 ($\delta^{34}S = 20.3‰$, Hut, 1987) and IAEA-SO-6 ($\delta^{34}S = -34.1‰$). The true value for NBS 127 may be higher, i.e. 21.1‰ (Halas and Szaran, 2001), which would mean that our values would need to be slightly corrected ($\delta^{34}S_{corr} = \delta^{34}S_{reported} \cdot 1.01 + 0.3$), which shifts our values maximally by 0.5‰, and does not affect the outcome of our study. The oxygen isotopic composition of sulfate and water is reported with respect to Vienna Standard Mean Ocean Water (VSMOW). The oxygen isotope measurements were calibrated with NBS 127 ($\delta^{18}O = 8.6‰$; Boschetti and Iacumin, 2005) and IAEA-SO-5 ($\delta^{18}O = 12.0‰$; Boschetti and Iacumin, 2005) and IAEA-SO-6 ($\delta^{18}O = -11.3‰$; Halas et al., 2007). The standard deviation of the measurements was less than 0.2‰ for $\delta^{34}S$ values and less than 0.3‰ for $\delta^{18}O$ values. The oxygen isotope composition of the experiment medium was determined via CO_2 equilibration and subsequent isotope analysis of CO_2 by GS-IRMS (Delta V, Finnigan; Thermo Fisher Scientific, Waltham, MA, USA) at the Geological Institute, ETH Zurich, Switzerland. The system was calibrated with the international reference waters SMOW, GISP and SLAP and the oxygen isotope ratios are reported in the δ-notation relative to VSMOW. The reproducibility of the measurements based on repeated measurements of standards is less than 0.1‰.

2.5. Calculation of SRR, $\varepsilon^{34}S$ and θ_O

Sulfate reduction rates and isotope fractionation values were calculated from mass and isotope balances, respectively. For calculations, steady state conditions were assumed. Sulfate reduction rates were quantified by either calculating sulfide production or sulfate consumption rates based on the mass conservation Eqs. (4) and (5), respectively.

$$SRR = D \cdot \left(\left[HS^-_{out} \right] - \left[HS^-_{in} \right] \right) \quad (4)$$

$$SRR = D \cdot \left(\left[SO^{2-}_{4\,in} \right] - \left[SO^{2-}_{4\,out} \right] \right) \quad (5)$$

Terms in brackets are concentration values for sulfate and sulfide in the inflow (in) and outflow (out) of the incubation vessel, respectively, whereas D is the hydraulic dilution rate (dimension: t^{-1}). Consequently, in continuous incubation at steady state, Eq. (6) should hold:

$$\left[HS^-_{out} \right] - \left[HS^-_{in} \right] = \left[SO^{2-}_{4\,in} \right] - \left[SO^{2-}_{4\,out} \right] \quad (6)$$

Under steady state conditions, the sulfur isotope composition of effluent sulfate and sulfide only depends on SRR (i.e. consumption of sulfate and production of sulfide within the reactor) and on the sulfur isotope enrichment factor by AOM-SR, i.e. $\varepsilon^{34}S$. The isotope enrichment factor, $\varepsilon^{34}S$, is related to the isotope fractionation factor $\alpha^{34}S$, which is commonly used in studies on sulfur isotope fractionation, according to Eq. (7).

$$\varepsilon^{34}S = 1000‰ \cdot \left(1 - \alpha^{34}S \right) \quad (7)$$

The value of $\varepsilon^{34}S$ was calculated according to Eq. (8) and Eq. (9) (for derivation see Supplementary Information). Data presented in this report consider averaged values calculated based on sulfate and sulfide mass balances from multiple measurements at steady state.

$$\varepsilon^{34}S \approx \delta^{34}S_{SO_{4\,out}^{2-}} - \delta^{34}S_{HS_{out}^{-}} + \frac{[HS_{in}^{-}]}{[HS_{out}^{-}] - [HS_{in}^{-}]} \cdot \left(\delta^{34}S_{HS_{in}^{-}} - \delta^{34}S_{HS_{out}^{-}}\right) \quad (8)$$

$$\varepsilon^{34}S \approx \frac{[SO_{4\,in}^{2-}]}{[SO_{4\,in}^{2-}] - [SO_{4\,out}^{2-}]} \cdot \left(\delta^{34}S_{SO_{4\,out}^{2-}} - \delta^{34}S_{SO_{4\,in}^{2-}}\right) \quad (9)$$

The bulk apparent oxygen isotope exchange between sulfate and water (AOM-Ex) mediated by AOM-SR is calculated according to Eq. (10).

$$\text{AOM-Ex} = D \cdot [SO_{4\,in}^{2-}] \cdot \frac{\delta^{18}O_{SO_{4\,out}^{2-}} - \delta^{18}O_{SO_{4\,in}^{2-}}}{\delta^{18}O_{water} + \varepsilon^{18}O_{H_2O \Leftrightarrow SO_4^{2-}} - \delta^{18}O_{SO_{4\,out}^{2-}}}, \quad (10)$$

where $\varepsilon^{18}O_{H_2O \Leftrightarrow SO_4^{2-}}$ corresponds to the oxygen isotope equilibrium fractionation between sulfate and water at 20 °C (~24‰, Zeebe, 2010). The oxygen isotope exchange parameter θ_O is defined according to Eq. (11) (Brunner et al., 2012).

$$\theta_O = \frac{\text{AOM-Ex}}{\text{SRR}} \quad (11)$$

2.6. Calculation of Gibbs free energies

Gibbs free energies of reaction (ΔG_r) were calculated based on energies of formation (Thauer et al., 1977) for overall AOM-SR (Eq. (1)). The following activity coefficients for ionic species were considered: SO_4^{2-}: 0.2, HCO_3^-: 0.7, HS^-: 0.6. The activity coefficient for aqueous CH_4 was calculated to be approximately 1.2. The effect of increased hydrostatic pressure (15 MPa) was considered in thermodynamic calculations.

2.7. Calculation of SRR_{bm}

Biomass specific SRR (SRR_{bm}, dimension mmol/g_{DW}/d) were calculated based on the initial biomass dry weight concentration of 4.6 g_{DW}/L. This procedure neglects biomass growth effects. Growth of organisms performing AOM-SR is generally slow (e.g. Nauhaus et al., 2007) and expected to be of minor importance for the observed isotope effects. Black Sea biomass performing AOM-SR is mainly constituted by large aggregates consisting of active biomass, inactive or non-AOM-SR cells, as well as extracellular polymeric substances and carbonate precipitates (Michaelis et al., 2002). Since biomass growth could not be measured directly in a robust way and biomass sampling from the high-pressure experimental system would have caused significant process disturbance and biomass loss, uncertainties were accounted for by showing a possible range of growth related changes of SRR_{bm}, as highlighted in Figs. 4 and 5, respectively. This range is calculated based on previous estimates for growth of biomass performing AOM-SR. Ambient to low pressure incubations found doubling times of 1.1–1.5 (Girguis et al., 2005), 3.8 (Meulepas et al., 2009) and 7 months (Nauhaus et al., 2007). Similar growth rates were also found for thermophilic cultures with a doubling time of 2.3 months (Holler et al., 2011b) and in high-pressure bioreactor studies (2.5 months, Zhang et al., 2011).

3. Results

This study reports $\varepsilon^{34}S$ and θ_O for a naturally enriched biomass actively catalyzing AOM-SR during a continuous incubation experiment where the concentration of aqueous methane was stepwise increased over 92 days from 1.4±0.6 mM to 58.8±10.5 mM, with intervals of stabilization between measurement periods (Fig. 3a).

3.1. Sulfate and sulfide concentration

During the course of our experiment, the offset in concentration of sulfate or sulfide between the inflow and outflow increases with increasing methane concentration (Fig. 3). Sulfate removal exceeded sulfide production by a factor of 1.9 relative to the expected 1:1 ratio (Eq. (3)) at highest SRR. Theoretically, sulfide and sulfate concentration balances are equally well suited as a measure for SRR under controlled incubation conditions (Eq. (6)), and both sulfide production and sulfate removal are considered in calculation of SRR and SRR_{bm} throughout this study. As a consequence, the variance in SRR_{bm} is large (Table 1, Figs. 4 and 5). We have not found any evidence that sulfide is lost or oxidized during fluid sampling or analysis. The samples were instantaneously fixed by the formation of ZnS to prevent sulfide oxidation during sampling. However, some effluent samples contained measurable amounts of zero-valent sulfur (up to 18%, on average 2.2% of measured sulfide). This amount of dissolved zero-valent sulfur alone cannot explain the deviations between sulfate and sulfide mass balance. Considering the low solubility of zero-valent sulfur and polysulfides (Kamyshny et al., 2004, 2006, 2007), it is likely that solid or biomass associated sulfur accumulated during the experiments, which may account for the discrepancy in the sulfur mass balance but was not analyzed in our experiments.

3.2. Isotope composition of sulfate and sulfide

The $\delta^{34}S$ values of influent and effluent sulfate and sulfide, as well as $\delta^{18}O$ values of influent and effluent sulfate are shown in Fig. 3. Our isotope data set shows two unexpected features. First, the $\delta^{34}S$ values of effluent sulfide at low methane concentrations are associated with a large variance. We attribute this large range to the mixing of the small amount of sulfide that was actually produced by AOM-SR at these low methane concentrations with sulfide from the medium, which was used as a reducing agent. Under these conditions, the scatter in the data is amplified by slight changes in the flow rate of medium through the reactor. At higher rates of AOM-SR (higher methane concentrations), the variance becomes small because the relatively small amount of sulfide from the medium does not affect the sulfur isotope signature in the sulfide of the outflow to a measurable degree. Secondly, in the last experimental step, at a methane concentration of approximately 60 mM, the $\delta^{34}S$ value and to a lesser extent the $\delta^{18}O$ value of sulfate from the inflow was high. This shift in the isotope composition does not have an effect for the subsequent calculation of $\varepsilon^{34}S$ and θ_O because the $\delta^{34}S$ and values $\delta^{18}O$ for effluent sulfate mirrored this change. Contamination of the medium reservoir with AOM-SR active biomass that would have altered the isotope composition of sulfate in the inflow is highly unlikely because of the extremely low growth rates of AOM consortia. Likely, the change in $\delta^{34}S$ and $\delta^{18}O$ of influent sulfate was caused by the use of a different stock sulfate when the medium for the experimental phase between 40 and 120 days was prepared.

3.3. $\varepsilon^{34}S$, AOM-Ex and θ_O

The calculated $\varepsilon^{34}S$, AOM-Ex and θ_O are shown in Figs. 4 and 5 as a function of methane concentration (Figs. 4a, 5a), biomass specific rate SRR_{bm} (Figs. 4b, 5b) and free energy yield ΔG_r (Figs. 4c, 5c). The large variance associated with the calculated maximum values for $\varepsilon^{34}S$ and θ_O are due to deviations in influent sulfide concentrations and low turnover rates at low methane concentrations, and in the case of $\varepsilon^{34}S$ also due to scatter in the $\delta^{34}S$ values of effluent sulfide. Changes in the concentrations of aqueous

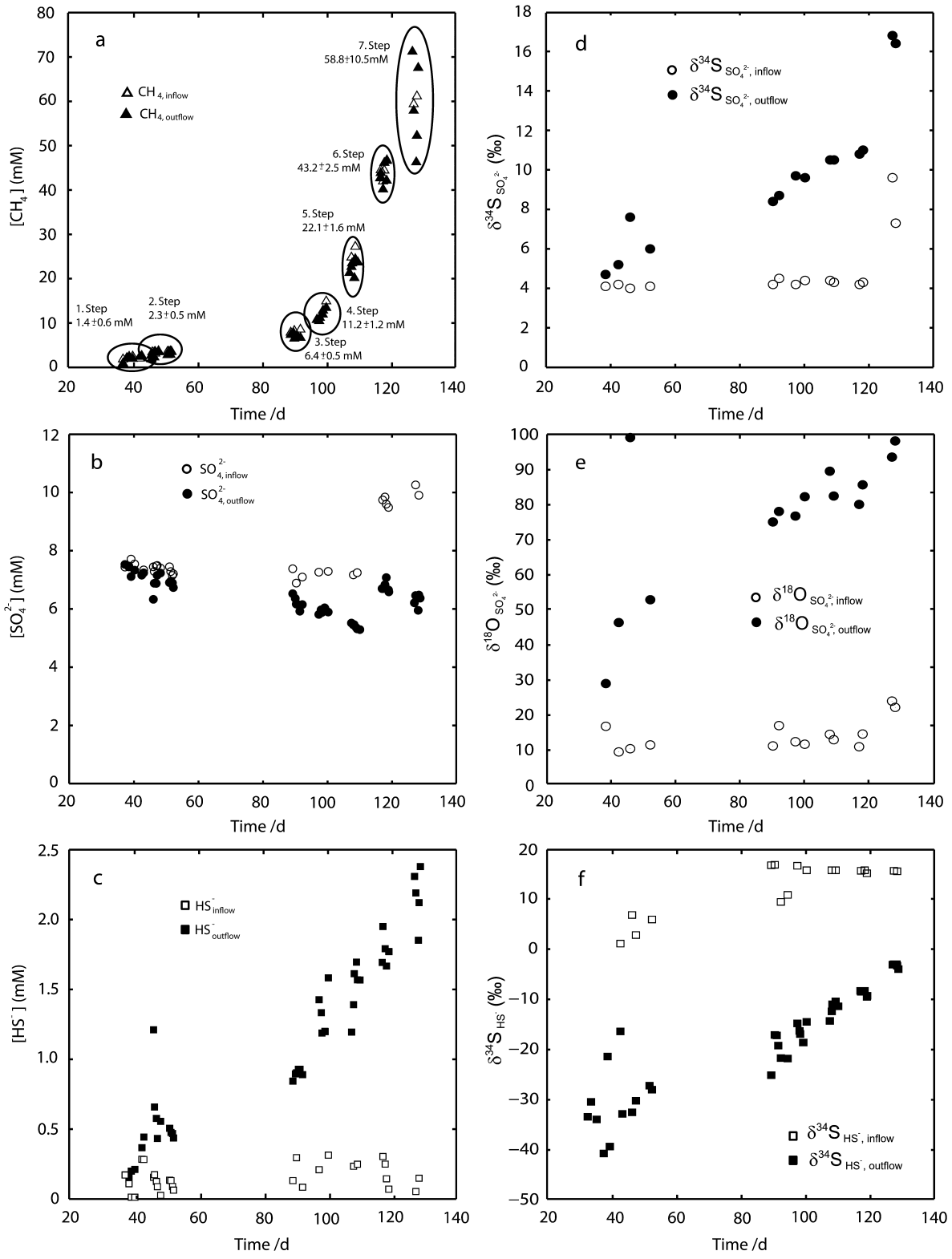

Fig. 3. Methane, sulfate and sulfide concentrations, $\delta^{34}S$ and $\delta^{18}O$ values of influent and effluent sulfate and sulfide during continuous incubation steps. Influent and effluent concentrations of (a) methane (b) sulfate, and (c) sulfide during seven incubation steps spanning the experimental period. Data are grouped representing single incubation steps at different methane concentrations (a, black ellipsoids). Data indicate that sulfate is consumed (b) and sulfide produced (c). Sulfide was present in the influent because sodium sulfide was used as reducing agent. Sulfur and oxygen isotope compositions of sulfate (d and e, respectively) show that effluent sulfate is enriched in the heavy isotopes ^{34}S and ^{18}O relative to influent sulfate. Effluent sulfide is depleted in ^{34}S relative to influent sulfide (f).

methane during AOM-SR coincide with strong changes in sulfate reduction rates, but also in AOM-Ex, $\varepsilon^{34}S$ and θ_O. We observe the highest SSR_{bm} and AOM-Ex at the highest methane concentrations, where $\varepsilon^{34}S$ and θ_O are lowest (21.9 ± 1.9‰ and 0.5 ± 0.2, respectively). The maximum values for $\varepsilon^{34}S$ of 67.3 ± 26.1‰ and θ_O of 2.5 ± 1.5 were observed at the lowest methane concentration, which coincide with the lowest sulfate reduction rates and AOM-Ex (Figs. 4, 5).

Table 1
Sulfate removal and sulfide production at different methane concentrations. $SRR_{sulfate}$ and $SRR_{sulfide}$ are volumetric rates calculated from differences in influent and effluent sulfate or sulfide concentrations, respectively (values are shown as arithmetic means ± SD, see also Table S1 in *Supplementary Information* for concentration values).

Step	Days	$[CH_4]$ (mM)	$SRR_{sulfate}$ (mmol L^{-1} d^{-1})	$SRR_{sulfide}$ (mmol L^{-1} d^{-1})	$SRR_{sulfate}/SRR_{sulfide}$ (/)
1	37–43	1.4 ± 0.6	0.2 ± 0.3	0.2 ± 0.2	1.0
2	46–52	2.3 ± 0.5	0.8 ± 0.3	0.7 ± 0.1	1.1
3	89–92	6.4 ± 0.5	1.6 ± 0.4	1.3 ± 0.1	1.2
4	97–100	11.2 ± 1.2	2.3 ± 0.2	1.8 ± 0.3	1.3
5	107–110	22.1 ± 1.6	3.1 ± 0.2	2.2 ± 0.3	1.4
6	117–119	43.2 ± 2.5	5.0 ± 0.3	2.7 ± 0.2	1.9
7	127–129	58.8 ± 10.5	6.5 ± 0.4	3.5 ± 0.4	1.9

4. Discussion

4.1. Relationship between $\varepsilon^{34}S$, θ_O, SRR_{bm}, energy yield and methane concentration

Small $\varepsilon^{34}S$ and θ_O coincide with high methane concentrations and relatively high energy yield, large $\varepsilon^{34}S$ and θ_O with low methane concentrations and low energy yield (Figs. 4a, c; 5a, c). However, $\varepsilon^{34}S$ and θ_O also correlate with SRR_{bm} (Figs. 4b; 5b), and conversely, SRR_{bm} correlate with methane concentrations and the calculated energy yield. This interrelation between all parameters is not unexpected for two reasons. First, $\varepsilon^{34}S$ and θ_O are expected to be a measure of the reversibility of AOM-SR, which should depend on the energy yield (for a simple enzymatically catalyzed reaction, see Eq. (2)). Second, the net sulfate consumption rate, SRR_{bm}, depends on the rate of individual enzymatically catalyzed reactions, which should depend on substrate and product concentrations as well (Eq. (3)). In principle, an organism could employ an increased number of enzymes to counteract low SRR_{bm} under low energy yield, however, this appears unlikely as maintaining a higher number of enzymes comes at additional energy cost.

4.2. Relationship between $\varepsilon^{34}S$ and θ_O for AOM-SR and comparison to DSR and sulfur disproportionation

We observe a strong correlation between $\varepsilon^{34}S$ and θ_O in AOM-SR, resonating the predictions – and to some extent observations – that such a correlation exists for the DSR pathway (Mangalo et al., 2007, 2008; Einsiedl, 2008; Turchyn et al., 2010; Brunner et al., 2012). The $\varepsilon^{34}S$–θ_O relationship for AOM-SR from our experiment covers almost the entire range of previously observed $\varepsilon^{34}S$–θ_O relationships for DSR, and even expands it to higher $\varepsilon^{34}S$ values (Fig. 6). Notably, our observed $\varepsilon^{34}S$–θ_O relationship for AOM-SR falls within the theoretical $\varepsilon^{34}S$–θ_O field for DSR predicted by Brunner et al. (2012).

It is interesting to discuss the observed $\varepsilon^{34}S$ and θ_O for AOM-SR in light of the finding that sulfur cycling by AOM-SR may consist of two interlinked processes – sulfate reduction to zero-valent sulfur by the ANME and sulfur disproportionation by the DSS (Milucka et al., 2012). The biochemical mechanistics and potential sulfur and oxygen isotope effects of the hypothesized sulfate reduction to zero-valent sulfur by the ANME are currently unknown, but some information about the mechanics of sulfur disproportionation utilized by the DSS partner and the associated isotope effects is available. It appears that sulfur disproportionation makes use of a partially reversed DSR pathway (Frederiksen and Finster, 2003; Finster et al., 2013) which implies that if this pathway is operated in a highly reversible manner, sulfur and oxygen isotope effects for sulfur disproportionation might be similar to those for DSR. Similar to the sulfur isotope effects by DSR, $\varepsilon^{34}S$ for the disproportionation of elemental sulfur to sulfate and sulfide depend on experimental conditions (i.e. type of provided sulfide scavenger) and culture-types, varying between ~0 and ~35‰ (Böttcher et al., 2005). If DSS in consortia responsible for AOM-SR operate more reversibly than these classical sulfur-disproportionating bacteria, even larger $\varepsilon^{34}S$ should occur. Although it cannot be excluded that DSS also contribute to overall sulfate reduction during AOM-SR via the canonical DSR pathway, it could be speculated that the similarity between the $\varepsilon^{34}S$–θ_O relationship for AOM-SR and DSR is mainly caused by the similarity of the biochemical mechanics of DSR and sulfur disproportionation, the latter overprinting potential sulfur and oxygen isotope effects related to sulfate reduction by ANME. Consequently, the overlap between $\varepsilon^{34}S$–θ_O relationships for AOM-SR and DSR does not imply that the processes are mechanistically identical. Rather, the implication is that the underlying principles of reversibility at low energy yields apply to both processes and that it may be difficult to disentangle DSR from AOM-SR based on $\varepsilon^{34}S$–θ_O relationships. Although theoretically the sulfur isotope effects for sulfate reduction by ANME and sulfur disproportionation by DSS could be staggered in analogy to what has been proposed for canonical DSR combined with sulfur disproportionation (Canfield and Thamdrup, 1994), the thermodynamic constraints on the overall AOM-SR process may be the reason why our observed maximum sulfur isotope fractionation did not exceed the maximum for the sulfur isotope fractionation between sulfate and sulfide of approximately 75‰. Studies targeting the multiple S isotope signature (^{32}S, ^{33}S, ^{34}S, ^{36}S) of AOM-SR have not been carried out yet, but may provide additional information that helps elucidating the mechanistic similarities and dissimilarities between DSR and AOM-SR.

4.3. Range of $\varepsilon^{34}S$ and θ_O for AOM-SR and application to natural systems

In our experiment on AOM-SR, we observed sulfur isotope fractionation as low as 21.9 ± 1.9‰, but also as high as 67.3 ± 26.1‰, thereby approaching the sulfur isotope equilibrium fractionation of approximately 75‰. Sulfur isotope fractionations exceeding 60‰ were also observed for a pure DSR culture grown on glucose by Sim et al. (2011a), who pointed out that such large fractionations are likely much more relevant for natural environments than the multitude of significantly lower $\varepsilon^{34}S$ found for various cultures of sulfate reducers grown in the laboratory on easily degradable substrates. This raises the question whether the values of $\varepsilon^{34}S$ and θ_O found in our steady-state experiments with a naturally enriched biomass performing AOM-SR are representative for the natural environment. We believe this is the case, as our experimental approach bridges pure culture studies and field measurements. From the strong dependency of $\varepsilon^{34}S$ and θ_O of AOM-SR on methane concentrations we conclude that there is a large variety of sulfur and oxygen isotope signatures for AOM-SR in natural systems, which depends on the methane availability (Fig. 6). We expect large $\varepsilon^{34}S$ and θ_O of AOM-SR where methane concentrations are low. A typical system where this occurs is in sediments where burial of organic matter is elevated to a degree that pore-water sulfate becomes depleted and methanogenesis produces methane

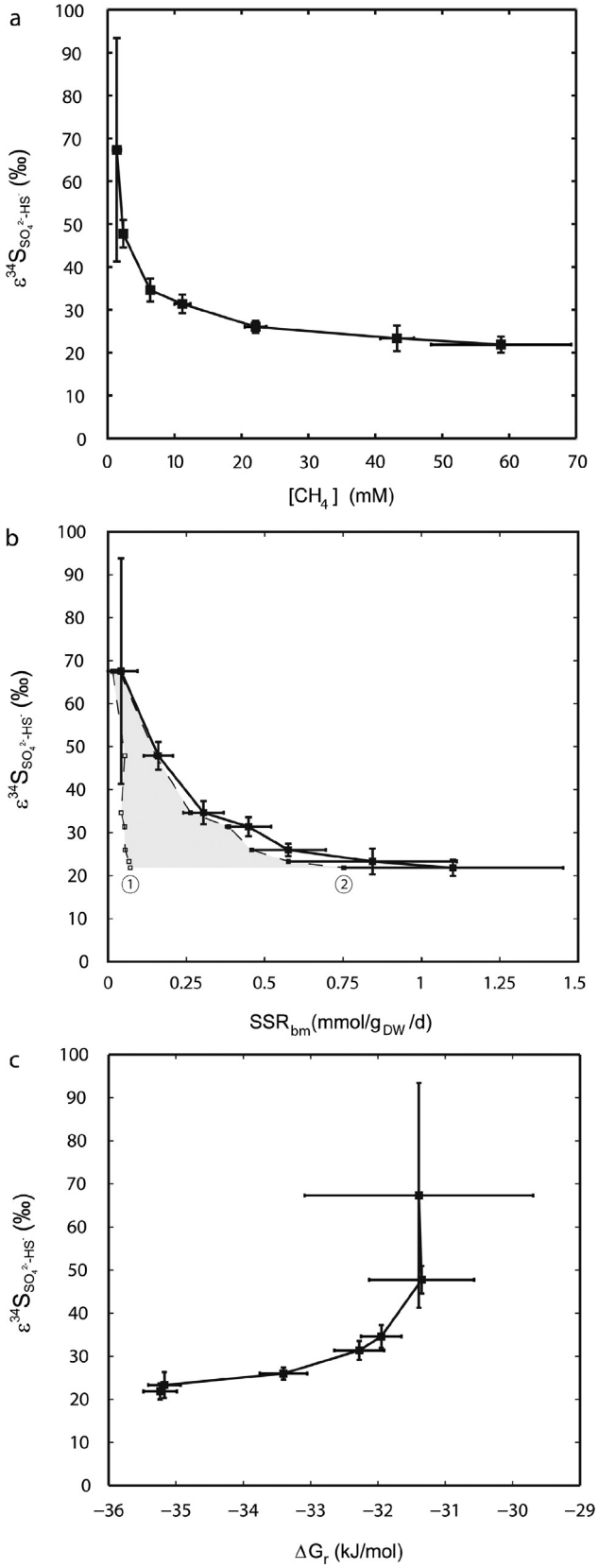

Fig. 4. Sulfur isotope fractionation ($\varepsilon^{34}S$) as a function of methane concentration, biomass specific rate, and Gibbs free energy yield. S-isotope fractionation values ($\varepsilon^{34}S$) are shown as a function of (a) methane concentration, (b) biomass specific rate (SRR_{bm}), and (c) Gibbs free energy yield (ΔG_r). Growth related uncertainties of SRR_{bm} are indicated by grey areas that span data regions assuming organism doubling times between 1 month (dashed line 1, Girguis et al., 2005), and 7 months (dashed line 2, Nauhaus et al., 2007). Data are plotted as arithmetic means ± SD.

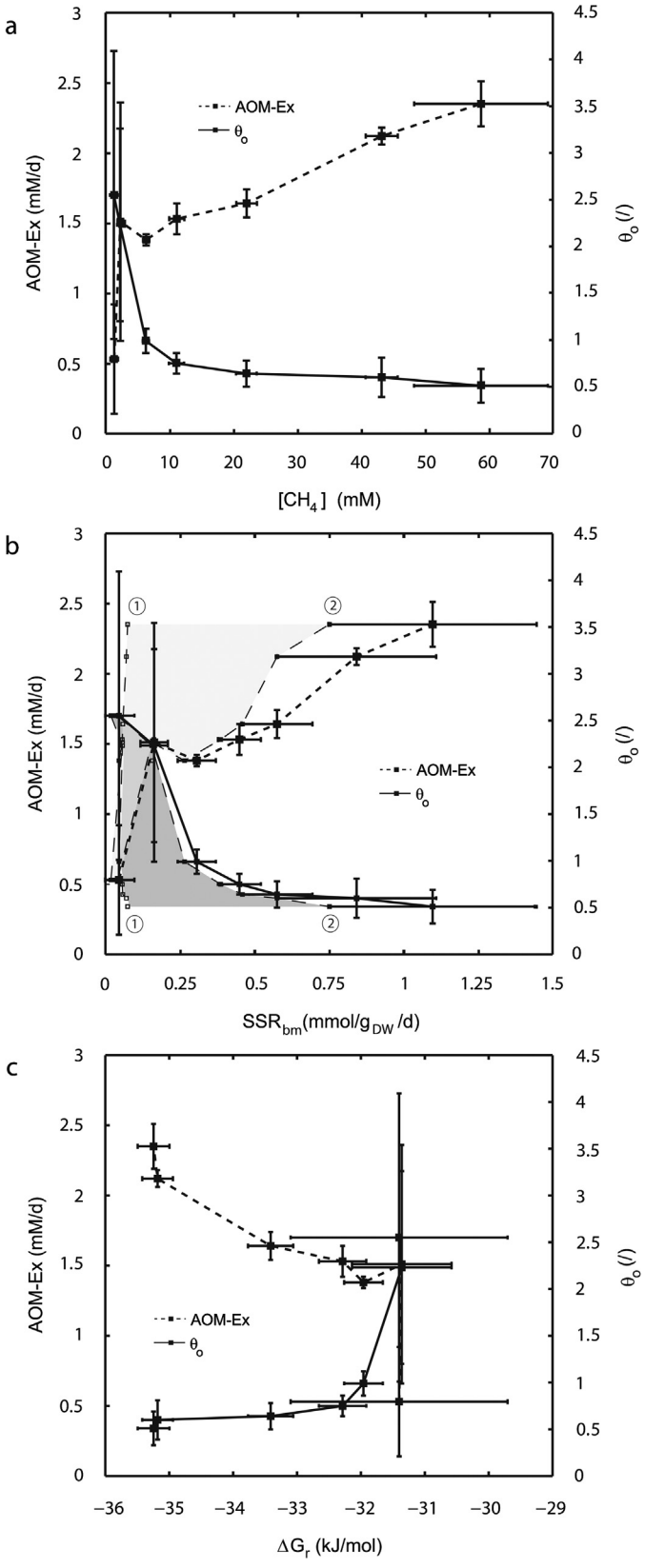

Fig. 5. Bulk apparent oxygen isotope exchange between sulfate and water mediated by AOM-SR and θ_O. The two parameters AOM-Ex and θ_O for AOM-SR are shown as a function of (a) methane concentration, (b) biomass specific rate (SRR_{bm}), and (c) Gibbs free energy yield (ΔG_r). Note, that SRR is used in the calculation of θ_O (Eq. (11)). Growth related uncertainties of SRR_{bm} are indicated by grey areas that span data regions assuming organism doubling times between 1 month (dashed lines 1, Girguis et al., 2005), and 7 months (dashed lines 2, Nauhaus et al., 2007). Data are plotted as arithmetic means ± SD.

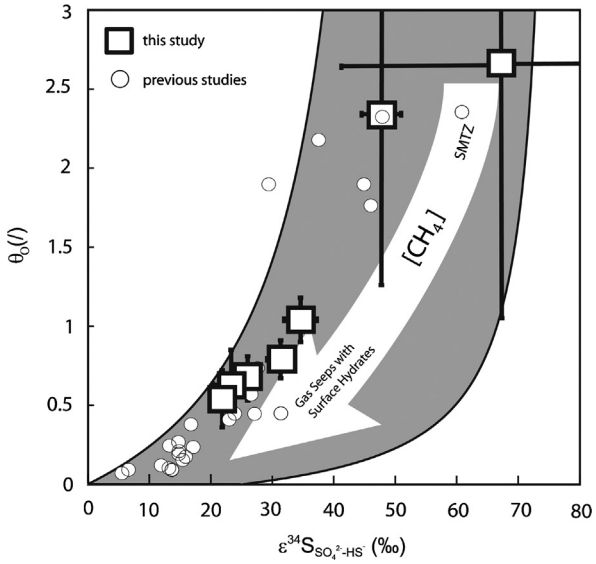

Fig. 6. Comparison of ε^{34}S–θ_O relationships of AOM-SR to ε^{34}S–θ_O relationships of DSR and to methane concentrations in selected marine environments. Relationship between ε^{34}S and θ_O for AOM-SR (open squares) and DSR (open circles). Our results fall within the range of ε^{34}S–θ_O relationships predicted for DSR based on a sulfur and oxygen isotope fractionation model (grey area; Brunner et al., 2012). The white arrow indicates the trend from high ε^{34}S and θ_O at low methane concentrations which are typical for SMTZs in marine sediments to low ε^{34}S and θ_O at high methane concentrations which are typical for gas seeps with surface hydrates. Data are plotted as arithmetic means ± SD. Additional information on maximum methane concentrations in marine environments as a function of pressure and temperature is provided in Supplementary Fig. S1.

from substrates no longer available to DSR. Such systems are typically diffusion controlled and result in the development of a SMTZ where AOM-SR maintains both low methane and sulfate concentrations (e.g. Iversen and Jørgensen, 1985). Typically, minimum methane concentrations in such systems are even below the lowest methane concentrations in our experiment (1.4 ± 0.6 mM, Fig. 3a), where we observe ε^{34}S to be as high as 67.3 ± 26.1‰. Indeed, large sulfur isotope offsets between sulfate and sulfide have been found for such systems, for example in the Black Sea (Jørgensen et al., 2004) and in the Cariaco Basin (Werne et al., 2003) with 59 to 77‰ and 53 to 65‰, respectively. However, numerous sites with high methane advection rates are also known, such as mud volcano and methane seep systems. Sediments at methane seep systems are often characterized by two-phase gas–water fluid transport and elevated concentrations of aqueous methane in equilibrium with free gas or gas hydrates (see Supplementary Fig. S1 for equilibrium concentrations) which coincide with substantial sulfate concentrations (Haeckel et al., 2004; Heeschen et al., 2007, 2011). In these environments small ε^{34}S and θ_O of AOM-SR would be expected. Mud volcano and seep systems are not only characterized by higher methane fluxes (e.g. Lichtschlag et al., 2010, and references therein), but also by rapid changes in fluxes (e.g. de Beer et al., 2006, and references therein). Considering that our enrichments of biomass performing AOM-SR quickly adapted to the changed methane concentrations we would also expect a higher variability of expressed ε^{34}S and θ_O. Special environments to consider may be locations where sulfate-rich water comes in contact with heterogeneously distributed gas hydrates (Boetius et al., 2000; Boetius and Suess, 2004) or where gas hydrates dissociate due to natural or anthropogenic changes in bottom water temperatures and increased amounts of methane are released (Bernd et al., 2014; Biastoch et al., 2011). In such a case, locally and temporarily elevated methane concentrations could increase AOM-SR and corresponding small sulfur isotope offsets between sulfate and sulfide, as well as small θ_O should be expected. As a consequence of the apparent metabolic capability to adapt to changing methane concentrations, signals from transient events with high methane availability might be imprinted in the S-isotope record and help to reconstruct past methane release events.

5. Conclusions

With naturally enriched, heterogeneous biomass that performs AOM-SR under controlled incubation conditions, we observe a strong dependency of ε^{34}S and θ_O on methane (substrate) concentration. This finding corroborates the hypothesis that weakly exergonic processes must be highly reversible – to a point where back flux of product to the substrate pool becomes possible (Holler et al., 2011a) – and that the extent of the reversibility, and as such the expression of isotope effects, is substrate concentration dependent. We have shown that naturally enriched active biomass performing AOM-SR is able to quickly adapt to changing substrate concentrations even at methane concentrations strongly exceeding concentrations in the natural habitat, implying the metabolic pathways that constitute AOM-SR allow for efficient use of available substrate by rapid adjustment of specific turnover rates. The presence of dissolved and extracellular zero-valent sulfur and the observation that sulfate consumption exceeds sulfide production in our experiment are consistent with the finding that zero-valent sulfur is likely an intermediate during AOM-SR and that sulfate consumption may be carried out by a different organism (i.e. ANME) than sulfide production (i.e. DSS; Milucka et al., 2012). This also raises the question if under our experimental conditions the growth and/or metabolic rate of ANME was slightly faster than the growth rate of their bacterial partners, leading to the accumulation of elemental sulfur in the reactor.

Under environmental conditions, AOM-SR is likely to induce a wide range of sulfur and oxygen isotope fractionations, depending on ambient methane concentrations. In sedimentary SMTZs where supply with methane is generally low, ε^{34}S resulting from AOM-SR are likely to exceed +50‰ and even approach the theoretical sulfur isotope equilibrium of +75‰, and to drive oxygen isotope enrichment of sulfate toward the sulfate–water oxygen isotope equilibrium value, which explains large sulfur isotope offsets between sulfate and sulfide from biologically active sulfate–methane transition zones. At methane gas seeps and locations where sulfate-rich water comes in contact with gas hydrates, ε^{34}S and θ_O are expected to be much smaller, and also more variable. Factors other than methane concentrations might have an impact on the sulfur and oxygen isotope effects by AOM-SR in the environment and to some extent on the results of our study. For example, increased steady state sulfide concentrations could affect isotope fractionation – either by affecting the overall energy yield of the reaction or by product inhibition and toxic effects on AOM-SR. As AOM-SR proceeds over a wide range of sulfide activities (e.g. Nauhaus et al., 2002) we assume that our enrichment cultures did not suffer from inhibitory effects due to sulfide stress. Because the detailed mechanistic coupling between methane oxidation and sulfate reduction during AOM-SR remains unknown, we believe that it would be valuable to conduct incubation experiments with changing concentrations of substrates (sulfate, methane) and products (sulfide, bicarbonate) in order to assess potential effects on the observed ε^{33}S, ε^{34}S and θ_O, due to changes in the overall energy yield, and, in the case of sulfate, also due to potential suppression of isotope effects at very low sulfate concentrations (Habicht et al., 2002). This approach could open an avenue to the reconstruction of the concentration of substrates and products of AOM-SR from the rock record, where pyrite minerals and carbonate-associated sulfate from diagenetic carbonates preserve such isotope signatures.

Acknowledgements

We thank Antje Boetius for providing the natural AOM enrichments (expedition Meteor M72/2) and for comments on an earlier version of the manuscript. We thank Kirsten Imhoff and Thomas Max for technical support. Matthias Haeckel and Elke Kossel have kindly provided program codes for thermodynamical calculations. We thank Doug LaRowe for support in calculation of pressure compensated Gibbs free energies. Gideon Henderson, Simon Bottrell and 2 anonymous reviewers are thanked for their comments that helped improve this manuscript greatly. Our project would not have been possible without the kind encouragement by T.G. Ferdelman and F. Widdel. This study was supported by the Max Planck Society and the R and D Program GEOTECHNOLOGIEN project MUMM II funded by the Federal Ministry of Education and Research (BMBF), Germany, Grant 03G0608C. This is publication No. GEOTECH-2198 of the program GEOTECHNOLOGIEN.

Appendix A. Supplementary material

Supplementary material related to this article can be found online at http://dx.doi.org/10.1016/j.epsl.2014.04.047.

References

Aeckersberg, F., Bak, F., Widdel, F., 1991. Anaerobic oxidation of saturated hydrocarbons to CO_2 by a new type of sulfate-reducing bacterium. Arch. Microbiol. 156, 5–14.

Aharon, P., Fu, B., 2000. Microbial sulfate reduction rates and sulfur and oxygen isotope fractionations at oil and gas seeps in deepwater Gulf of Mexico. Geochim. Cosmochim. Acta 64, 233–246.

Aharon, P., Fu, B., 2003. Sulfur and oxygen isotopes of coeval sulfate–sulfide in pore fluids of cold seep sediments with sharp redox gradients. Chem. Geol. 195, 201–218.

Antler, G., Turchyn, A.V., Rennie, V., Herut, B., Sivan, O., 2013. Coupled sulfur and oxygen isotope insight into bacterial sulfate reduction in the natural environment. Geochim. Cosmochim. Acta 118, 98–117. http://dx.doi.org/10.1016/j.gca.2013.1005.1005.

Arnds, J., 2009. Molecular Characterization of Microbial Populations in Methane-Rich Marine Habitats. University Bremen, Bremen.

Arning, E.T., Birgel, D., Brunner, B., Peckmann, J., 2009. Bacterial formation of phosphatic laminites off Peru. Geobiology 7, 295–307.

Balci, N., Shanks III, W.C., Mayer, B., Mandernack, K.W., 2007. Oxygen and sulfur isotope systematics of sulfate produced by bacterial and abiotic oxidation of pyrite. Geochim. Cosmochim. Acta 71, 3796–3811.

Bao, H., 2006. Purifying barite for oxygen isotope measurement by dissolution and reprecipitation in a chelating solution. Anal. Chem. 78, 304–309.

Basen, M., Krüger, M., Milucka, J., Kuever, J., Kahnt, J., Grundmann, O., Meyerdierks, A., Widdel, F., Shima, S., 2011. Bacterial enzymes for dissimilatory sulfate reduction in a marine microbial mat (Black Sea) mediating anaerobic oxidation of methane. Environ. Microbiol. 13, 1370–1379.

Berndt, C., Feseker, T., Treude, T., Krastel, S., Liebetrau, V., Niemann, H., Bertics, V.J., Dumke, I., Dunnbier, K., Ferre, B., Graves, C., Gross, F., Hissmann, K., Huhnerbach, V., Krause, S., Lieser, K., Schauer, J., Steinle, L., 2014. Temporal constraints on hydrate-controlled methane seepage off Svalbard. Science 343, 284–287.

Berner, R.A., Petsch, S.T., Lake, J.A., Beerling, D.J., Popp, B.N., Lane, R.S., Laws, E.A., Westley, M.B., Cassar, N., Woodward, F.I., Quick, W.P., 2000. Isotope fractionation and atmospheric oxygen: implications for Phanerozoic O_2 evolution. Science 287, 1630–1633.

Biastoch, A., Treude, T., Rüpke, L.H., Riebesell, U., Roth, C., Burwicz, E.B., Park, W., Latif, M., Böning, C.W., Madec, G., Wallmann, K., 2011. Rising Arctic Ocean temperatures cause gas hydrate destabilization and ocean acidification. Geophys. Res. Lett. 38, L08602.

Boetius, A., Suess, E., 2004. Hydrate ridge: a natural laboratory for the study of microbial life fueled by methane from near-surface gas hydrates. Chem. Geol. 205, 291–310.

Boetius, A., Ravenschlag, K., Schubert, C.J., Rickert, D., Widdel, F., Gieseke, A., Amann, R., Jørgensen, B.B., Witte, U., Pfannkuche, O., 2000. A marine microbial consortium apparently mediating anaerobic oxidation of methane. Nature 407, 623–626.

Borowski, W.S., Rodriguez, N.M., Paull, C.K., Ussler III, W., 2013. Are ^{34}S-enriched authigenic sulfide minerals a proxy for elevated methane flux and gas hydrates in the geologic record? Mar. Pet. Geol. 43, 381–395.

Boschetti, T., Iacumin, P., 2005. Continuous-flow δ^{18}O measurements: new approach to standardization, high-temperature thermodynamic and sulfate analysis. Rapid Commun. Mass Spectrom. 19, 3007–3014.

Böttcher, M.E., Thamdrup, B., 2001. Anaerobic sulfide oxidation and stable isotope fractionation associated with bacterial sulfur disproportionation in the presence of MnO_2. Geochim. Cosmochim. Acta 65, 1573–1581.

Böttcher, M.E., Brumsack, H.J., de Lange, G.J., 1998. Sulfate reduction and related stable isotope (^{34}S, ^{18}O) variations in interstitial waters from the eastern Mediterranean. Proc. ODP Sci. Res. 160, 365–373.

Böttcher, M.E., Bernasconi, S.M., Brumsack, H.J., 1999. Carbon, sulfur and oxygen isotope geochemistry of interstitial waters from the west Mediterranean. Proc. ODP Sci. Res. 161, 413–421.

Böttcher, M.E., Thamdrup, B., Vennemann, T.W., 2001. Oxygen and sulfur isotope fractionation during anaerobic bacterial disproportionation of elemental sulfur. Geochim. Cosmochim. Acta 65, 1601–1609.

Böttcher, M.E., Boetius, A., Rickert, D., 2003. Sulfur isotope fractionation during microbial sulfate reduction associated with anaerobic methane oxidation. TERRA NOSTRA 89.

Böttcher, M.E., Thamdrup, B., Gehre, M., Theune, A., 2005. S-34/S-32 and O-18/O-16 fractionation during sulfur disproportionation by Desulfobulbus propionicus. Geomicrobiol. J. 22, 219–226.

Bottrell, S.H., Newton, R.J., 2006. Reconstruction of changes in global sulfur cycling from marine sulfate isotopes. Earth-Sci. Rev. 75, 59–83.

Bottrell, S.H., Parkes, R.J., Cragg, B.A., Raiswell, R., 2000. Isotopic evidence for anoxic pyrite oxidation and stimulation of bacterial sulphate reduction in marine sediments. J. Geol. Soc. 157, 711–714.

Bradley, A.S., Leavitt, W.D., Johnston, D.T., 2011. Revisiting the dissimilatory sulfate reduction pathway. Geobiology 9, 446–457.

Brüchert, V., 2004. Physiological and ecological aspects of sulfur isotope fractionation during bacterial sulfate reduction. In: Amend, J.P., Edwards, K.J., Lyons, T.W. (Eds.), Sulfur Biogeochemistry – Past and Present. Geological Society of America, pp. 1–16.

Brunner, B., Bernasconi, S.M., 2005. A revised isotope fractionation model for dissimilatory sulfate reduction in sulfate reducing bacteria. Geochim. Cosmochim. Acta 69, 4759–4771.

Brunner, B., Bernasconi, S.M., Kleikemper, J., Schroth, M.H., 2005. A model for oxygen and sulfur isotope fractionation in sulfate during bacterial sulfate reduction processes. Geochim. Cosmochim. Acta 69, 4773–4785.

Brunner, B., Yu, J.-Y., Mielke, R.E., MacAskill, J.A., Madzunkov, S., McGenity, T.J., Coleman, M., 2008. Different isotope and chemical patterns of pyrite oxidation related to lag and exponential growth phases of Acidithiobacillus ferrooxidans reveal a microbial growth strategy. Earth Planet. Sci. Lett. 270, 63–72.

Brunner, B., Einsiedl, F., Arnold, G.L., Müller, I.A., Templer, S., Bernasconi, S.M., 2012. The reversibility of dissimilatory sulphate reduction and the cell-internal multi-step reduction of sulphite to sulphide: insights from the oxygen isotope composition of sulphate. Isot. Environ. Health Stud. 48, 33–54.

Burdett, J.W., Arthur, M.A., Richardson, M., 1989. A Neogene seawater sulfur isotope age curve from calcareous pelagic microfossils. Earth Planet. Sci. Lett. 94, 189–198.

Canfield, D.E., 2001. Biogeochemistry of sulfur isotopes. Rev. Mineral. Geochem. 43, 607–636.

Canfield, D.E., Teske, A., 1996. Late Proterozoic rise in atmospheric oxygen concentration inferred from phylogenetic and sulphur-isotope studies. Nature 382, 127–132.

Canfield, D.E., Thamdrup, B., 1994. The production of ^{34}S-depleted sulfide during bacterial disproportionation of elemental sulfur. Science 266, 1973–1975.

Chambers, L.A., Trudinger, P.A., 1979. Microbiological fractionation of stable sulfur isotopes – review and critique. Geomicrobiol. J. 1, 249–293.

Chambers, L.A., Trudinger, P.A., Smith, J.W., Burns, M.S., 1975. Fractionation of sulfur isotopes by continuous cultures of Desulfovibrio-desulfuricans. Can. J. Microbiol. 21, 1602–1607.

de Beer, D., Sauter, E., Niemann, H., Kaul, N., Foucher, J.P., Witte, U., Schluter, M., Boetius, A., 2006. In situ fluxes and zonation of microbial activity in surface sediments of the Haakon Mosby Mud Volcano. Limnol. Oceanogr. 51, 1315–1331.

Detmers, J., Brüchert, V., Habicht, K.S., Kuever, J., 2001. Diversity of sulfur isotope fractionations by sulfate-reducing prokaryotes. Appl. Environ. Microbiol. 67, 888–894.

Deusner, C., Meyer, V., Ferdelman, T.G., 2010. High-pressure systems for gas-phase free continuous incubation of enriched marine microbial communities performing anaerobic oxidation of methane. Biotechnol. Bioeng. 105, 524–533.

Einsiedl, F., 2008. Effect of NO_2^- on stable isotope fractionation during bacterial sulfate reduction. Environ. Sci. Technol. 43, 82–87.

Farquhar, J., Bao, H., Thiemens, M., 2000. Atmospheric influence of Earth's earliest sulfur cycle. Science 289, 756–758.

Farquhar, J., Canfield, D.E., Masterson, A., Bao, H., Johnston, D.T., 2008. Sulfur and oxygen isotope study of sulfate reduction in experiments with natural populations from Fællestrand, Denmark. Geochim. Cosmochim. Acta 72, 2805–2821.

Finster, K.W., Kjeldsen, K.U., Kube, M., Reinhardt, R., Mussmann, M., Amann, R., Schreiber, L., 2013. Complete genome sequence of Desulfocapsa sulfexigens, a marine deltaproteobacterium specialized in disproportionating inorganic sulfur compounds. Stand. Genomic Sci. 8, 58–68.

Frederiksen, T.-M., Finster, K., 2003. Sulfite-oxido-reductase is involved in the oxidation of sulfite in Desulfocapsa sulfoexigens during disproportionation of thiosulfate and elemental sulfur. Biodegradation 14, 189–198.

Fritz, P., Basharmal, G.M., Drimmie, R.J., Ibsen, J., Qureshi, R.M., 1989. Oxygen isotope exchange between sulphate and water during bacterial reduction of sulphate. Chem. Geol. 79, 99–105.

Girguis, P.R., Cozen, A.E., DeLong, E.F., 2005. Growth and population dynamics of anaerobic methane-oxidizing archaea and sulfate-reducing bacteria in a continuous-flow bioreactor. Appl. Environ. Microbiol. 71, 3725–3733.

Habicht, K.S., Gade, M., Thamdrup, B., Berg, P., Canfield, D.E., 2002. Calibration of sulfate levels in the Archean ocean. Science 298, 2372–2374.

Haeckel, M., Suess, E., Wallmann, K., Rickert, D., 2004. Rising methane gas bubbles form massive hydrate layers at the seafloor. Geochim. Cosmochim. Acta 68, 4335–4345.

Halas, S., Szaran, J., 2001. Improved thermal decomposition of sulfates to SO_2 and mass spectrometric determination of delta S-34 of IAEA SO-5, IAEA SO-6 and NBS-127 sulfate standards. Rapid Commun. Mass Spectrom. 15, 1618–1620.

Halas, S., Szaran, J., Czarnacki, M., Tanweer, A., 2007. Refinements in $BaSO_4$ to CO_2 preparation and $\delta^{18}O$ calibration of the sulfate reference materials NBS-127, IAEA SO-5 and IAEA SO-6. Geostand. Geoanal. Res. 31, 61–68.

Harrison, A., Thode, H., 1958. Mechanism of the bacterial reduction of sulphate from isotope fractionation studies. Trans. Faraday Soc. 54, 84–92.

Heeschen, K.U., Hohnberg, H.J., Haeckel, M., Abegg, F., Drews, M., Bohrmann, G., 2007. In situ hydrocarbon concentrations from pressurized cores in surface sediments, Northern Gulf of Mexico. Mar. Chem. 107, 498–515.

Heeschen, K.U., Haeckel, M., Klaucke, I., Ivanov, M.K., Bohrmann, G., 2011. Quantifying in-situ gas hydrates at active seep sites in the eastern Black Sea using pressure coring technique. Biogeosciences 8, 3555–3565.

Heidel, C., Tichomirowa, M., 2011. The isotopic composition of sulfate from anaerobic and low oxygen pyrite oxidation experiments with ferric iron – new insights into oxidation mechanisms. Chem. Geol. 281, 305–316.

Holler, T., Wegener, G., Niemann, H., Deusner, C., Ferdelman, T.G., Boetius, A., Brunner, B., Widdel, F., 2011a. Carbon and sulfur back flux during anaerobic microbial oxidation of methane and coupled sulfate reduction. Proc. Natl. Acad. Sci. USA 108, E1484–E1490.

Holler, T., Widdel, F., Knittel, K., Amann, R., Kellermann, M.Y., Hinrichs, K.-U., Teske, A., Boetius, A., Wegener, G., 2011b. Thermophilic anaerobic oxidation of methane by marine microbial consortia. ISME J. 5, 1946–1956.

Hut, G., 1987. Consultants' group meeting on stable isotope reference samples for geochemical and hydrological investigations. Report to the Director General. International Atomic Energy Agency, Vienna.

Iversen, N., Jørgensen, B.B., 1985. Anaerobic methane oxidation rates at the sulfate–methane transition in marine sediments from Kattegat and Skagerrak (Denmark). Limnol. Oceanogr. 30, 944–955.

Johnston, D.T., Wing, B.A., Farquhar, J., Kaufman, A.J., Strauss, H., Lyons, T.W., Kah, L.C., Canfield, D.E., 2005. Active microbial sulfur disproportionation in the Mesoproterozoic. Science 310, 1477–1479.

Johnston, D.T., Farquhar, J., Canfield, D.E., 2007. Sulfur isotope insights into microbial sulfate reduction: when microbes meet models. Geochim. Cosmochim. Acta 71, 3929–3947.

Jørgensen, B.B., Böttcher, M.E., Lüschen, H., Neretin, L.N., Volkov, I.I., 2004. Anaerobic methane oxidation and a deep H_2S sink generate isotopically heavy sulfides in Black Sea sediments. Geochim. Cosmochim. Acta 68, 2095–2118.

Kampschulte, A., Bruckschen, P., Strauss, H., 2001. The sulphur isotopic composition of trace sulphates in Carboniferous brachiopods: implications for coeval seawater, correlation with other geochemical cycles and isotope stratigraphy. Chem. Geol. 175, 149–173.

Kamyshny, A., Goifman, A., Gun, J., Rizkov, D., Lev, O., 2004. Equilibrium distribution of polysulfide ions in aqueous solutions at 25 °C: a new approach for the study of polysulfides' equilibria. Environ. Sci. Technol. 38, 6633–6644.

Kamyshny, A., Ekeltchik, I., Gun, J., Lev, O., 2006. Method for the determination of inorganic polysulfide distribution in aquatic systems. Anal. Chem. 78, 2631–2639.

Kamyshny, A., Gun, J., Rizkov, D., Voitsekovski, T., Lev, O., 2007. Equilibrium distribution of polysulfide ions in aqueous solutions at different temperatures by rapid single phase derivatization. Environ. Sci. Technol. 41, 2395–2400.

Kleikemper, J., Schroth, M.H., Bernasconi, S.M., Brunner, B., Zeyer, J., 2004. Sulfur isotope fractionation during growth of sulfate-reducing bacteria on various carbon sources. Geochim. Cosmochim. Acta 68, 4891–4904.

Knittel, K., Boetius, A., 2009. Anaerobic oxidation of methane: progress with an unknown process. Annu. Rev. Microbiol. 63, 311–334.

Knöller, K., Vogt, C., Richnow, H.-H., Weise, S.M., 2006. Sulfur and oxygen isotope fractionation during benzene, toluene, ethyl benzene, and xylene degradation by sulfate-reducing bacteria. Environ. Sci. Technol. 40, 3879–3885.

Knöller, K., Vogt, C., Feisthauer, S., Weise, S.M., Weiss, H., Richnow, H.-H., 2008. Sulfur cycling and biodegradation in contaminated aquifers: insights from stable isotope investigations. Environ. Sci. Technol. 42, 7807–7812.

Ku, T.C.W., Walter, L.M., Coleman, M.L., Blake, R.E., Martini, A.M., 1999. Coupling between sulfur recycling and syndepositional carbonate dissolution: evidence from oxygen and sulfur isotope composition of pore water sulfate, South Florida Platform, USA. Geochim. Cosmochim. Acta 63, 2529–2546.

Leavitt, W.D., Halevy, I., Bradley, A.S., Johnston, D.T., 2013. Influence of sulfate reduction rates on the Phanerozoic sulfur isotope record. Proc. Natl. Acad. Sci. USA 110, 11244–11249.

Lichtschlag, A., Felden, J., Wenzhöfer, F., Schubotz, F., Ertefai, T.F., Boetius, A., de Beer, D., 2010. Methane and sulfide fluxes in permanent anoxia: in situ studies at the Dvurechenskii mud volcano (Sorokin Trough, Black Sea). Geochim. Cosmochim. Acta 74, 5002–5018.

Mangalo, M., Meckenstock, R.U., Stichler, W., Einsiedl, F., 2007. Stable isotope fractionation during bacterial sulfate reduction is controlled by reoxidation of intermediates. Geochim. Cosmochim. Acta 71, 4161–4171.

Mangalo, M., Einsiedl, F., Meckenstock, R.U., Stichler, W., 2008. Influence of the enzyme dissimilatory sulfite reductase on stable isotope fractionation during sulfate reduction. Geochim. Cosmochim. Acta 72, 1513–1520.

Meulepas, R.J.W., Jagersma, C.G., Gieteling, J., Buisman, C.J.N., Stams, A.J.M., Lens, P.N.L., 2009. Enrichment of anaerobic methanotrophs in sulfate-reducing membrane bioreactors. Biotechnol. Bioeng. 104, 458–470.

Michaelis, W., Seifert, R., Nauhaus, K., Treude, T., Thiel, V., Blumenberg, M., Knittel, K., Gieseke, A., Peterknecht, K., Pape, T., Boetius, A., Amann, R., Jørgensen, B.B., Widdel, F., Peckmann, J., Pimenov, N.V., Gulin, M.B., 2002. Microbial reefs in the Black Sea fueled by anaerobic oxidation of methane. Science 297, 1013–1015.

Milucka, J., Ferdelman, T.G., Polerecky, L., Franzke, D., Wegener, G., Schmid, M., Lieberwirth, I., Wagner, M., Widdel, F., Kuypers, M.M.M., 2012. Zero-valent sulphur is a key intermediate in marine methane oxidation. Nature 491, 541–546.

Mizutani, Y., Rafter, T.A., 1969. Oxygen isotopic composition of sulphates – Part 4: bacterial fractionation of oxygen isotopes in the reduction of sulphate and in the oxidation of sulphur. N. Z. J. Sci. 12, 60–68.

Müller, I.A., Brunner, B., Coleman, M., 2013. Isotopic evidence of the pivotal role of sulfite oxidation in shaping the oxygen isotope signature of sulfate. Chem. Geol. 354, 186–202.

Nauhaus, K., Boetius, A., Krüger, M., Widdel, F., 2002. In vitro demonstration of anaerobic oxidation of methane coupled to sulphate reduction in sediment from a marine gas hydrate area. Environ. Microbiol. 4, 296–305.

Nauhaus, K., Albrecht, M., Elvert, M., Boetius, A., Widdel, F., 2007. In vitro cell growth of marine archaeal–bacterial consortia during anaerobic oxidation of methane with sulfate. Environ. Microbiol. 9, 187–196.

Ohkouchi, N., Kawamura, K., Kajiwara, Y., Wada, E., Okada, M., Kanamatsu, T., Taira, A., 1999. Sulfur isotope records around Livello Bonarelli (northern Apennines, Italy) black shale at the Cenomanian–Turonian boundary. Geology 27, 535–538.

Ono, S., Beukes, N., Sumner, D., Eigenbrode, J., Wing, B., Johnston, D., Farquhar, J., Rumble, D., 2005. Before the rise of oxygen: multiple sulfur isotope systematics in the late Archean basins in South Africa and Australia. Geochim. Cosmochim. Acta, Suppl. 69, A447.

Paytan, A., Kastner, M., Campbell, D., Thiemens, M.H., 1998. Sulfur isotopic composition of Cenozoic seawater sulfate. Science 282, 1459–1462.

Paytan, A., Kastner, M., Campbell, D., Thiemens, M.H., 2004. Seawater sulfur isotope fluctuations in the Cretaceous. Science 304, 1663–1665.

Philippot, P., Van Zuilen, M., Lepot, K., Thomazo, C., Farquhar, J., Van Kranendonk, M.J., 2007. Early Archaean microorganisms preferred elemental sulfur, not sulfate. Science 317, 1534–1537.

Pierre, C., 1985. Isotopic evidence for the dynamic redox cycle of dissolved sulfur-compounds between free and interstitial solutions in marine salt pans. Chem. Geol. 53, 191–196.

Pirlet, H., Wehrmann, L.M., Brunner, B., Frank, N., Dewanckele, J.A.N., Van Rooij, D., Foubert, A., Swennen, R., Naudts, L., Boone, M., Cnudde, V., Henriet, J.-P., 2010. Diagenetic formation of gypsum and dolomite in a cold-water coral mound in the Porcupine Seabight, off Ireland. Sedimentology 57, 786–805.

Reeburgh, W.S., 2007. Oceanic methane biogeochemistry. Chem. Rev. 107, 486–513.

Rees, C.E., 1973. A steady-state model for sulphur isotope fractionation in bacterial reduction processes. Geochim. Cosmochim. Acta 37, 1141–1162.

Riedinger, N., Brunner, B., Formolo, M.J., Solomon, E., Kasten, S., Strasser, M., Ferdelman, T.G., 2010. Oxidative sulfur cycling in the deep biosphere of the Nankai Trough, Japan. Geology 38, 851–854.

Shen, Y., Farquhar, J., Masterson, A., Kaufman, A.J., Buick, R., 2009. Evaluating the role of microbial sulfate reduction in the early Archean using quadruple isotope systematics. Earth Planet. Sci. Lett. 279, 383–391.

Sim, M.S., Bosak, T., Ono, S., 2011a. Large sulfur isotope fractionation does not require disproportionation. Science 333, 74–77.

Sim, M.S., Ono, S., Donovan, K., Templer, S.P., Bosak, T., 2011b. Effect of electron donors on the fractionation of sulfur isotopes by a marine Desulfovibrio sp. Geochim. Cosmochim. Acta 75, 4244–4259.

Strauss, H., Banerjee, D.M., Kumar, V., 2001. The sulfur isotopic composition of Neoproterozoic to early Cambrian seawater – evidence from the cyclic Hanseran evaporites, NW India. Chem. Geol. 175, 17–28.

Thauer, R.K., Jungermann, K., Decker, K., 1977. Energy conservation in chemotrophic anaerobic bacteria. Bacteriol. Rev. 41, 100–180.

Turchyn, A.V., Schrag, D.P., 2004. Oxygen isotope constraints on the sulfur cycle over the past 10 million years. Science 303, 2004–2007.

Turchyn, A.V., Brüchert, V., Lyons, T.W., Engel, G.S., Balci, N., Schrag, D.P., Brunner, B., 2010. Kinetic oxygen isotope effects during dissimilatory sulfate reduction: a combined theoretical and experimental approach. Geochim. Cosmochim. Acta 74, 2011–2024.

Werne, J.P., Lyons, T.W., Hollander, D.J., Formolo, M.J., Sinninghe Damsté, J.S., 2003. Reduced sulfur in euxinic sediments of the Cariaco Basin: sulfur isotope constraints on organic sulfur formation. Chem. Geol. 195, 159–179.

Widdel, F., Bak, F., 1992. Gram-negative mesophilic sulfate-reducing bacteria. In: Balows, A., Trüper, H.G., Dworkin, M., Harder, W., Schleifer, K.-H. (Eds.), The Prokaryotes. 2nd ed. Springer, New York, pp. 3352–3378.

Wortmann, U.G., Chernyavsky, B.M., 2007. Effect of evaporite deposition on Early Cretaceous carbon and sulphur cycling. Nature 446, 654–656.

Wortmann, U.G., Chernyavsky, B., Bernasconi, S.M., Brunner, B., Böttcher, M.E., Swart, P.K., 2007. Oxygen isotope biogeochemistry of pore water sulfate in the deep biosphere: dominance of isotope exchange reactions with ambient water during microbial sulfate reduction (ODP Site 1130). Geochim. Cosmochim. Acta 71, 4221–4232.

Yoshinaga, M.Y., Holler, T., Goldhammer, T., Wegener, G., Pohlmann, J.W., Brunner, B., Kuypers, M.M.M., Hinrichs, K.-U., Elvert, M., 2014. Carbon isotope equilibration during sulphate-limited anaerobic oxidation of methane. Nat. Geosci. 7, 190–194. http://dx.doi.org/10.1038/ngeo2069.

Zeebe, R.E., 2010. A new value for the stable oxygen isotope fractionation between dissolved sulfate ion and water. Geochim. Cosmochim. Acta 74, 818–828.

Zhang, Y., Maignien, L., Zhao, X., Wang, F., Boon, N., 2011. Enrichment of a microbial community performing anaerobic oxidation of methane in a continuous high-pressure bioreactor. BMC Microbiol. 11, 137.